Investigations of castellated structures for ITER: the effect of castellation shaping and alignment on fuel retention and impurity deposition in gaps

A. Litnovsky[1], P. Wienhold[1], V. Philipps[1], K. Krieger[2], A. Kirschner[1], D. Matveev[3], D. Borodin[1], G. Sergienko[1], O. Schmitz[1], A. Kreter[1], U. Samm[1], S.Richter[4], U. Breuer[5], J. P. Gunn[6], M. Komm[7], Z. Pekarek[7] and TEXTOR Team

[1]*Institut für Energieforschung - Plasmaphysik, Forschungszentrum Jülich, Trilateral Euregio Cluster, Association EURATOM- FZ Jülich, D-52425 Jülich, Germany;*

[2] *Max-Planck-Institut für Plasmaphysik, D-85748, Garching, Germany;*

[3]*Ghent University, Trilateral Euregio Cluster, Rozier B-9000, Ghent, Belgium*

[4]*Gemeinschaftslabor für Elektronenmikroskopie, RWTH Aachen, D-52056, Aachen, Germany;*

[5]*Zentralabteilung für Chemische Analysen, Forschungszentrum Jülich, D-52425, Jülich, Germany;*

[6]*Association Euratom-CEA, CEA/DSM/DRFC, Centre de Cadarache, 13108, Saint-Paul-Lez-Durance, France;*

[7] *Charles University in Prague, Faculty of Mathematics and Physics, Czech Republic.*

Abstract

Castellation will be used in divertor and first wall components to provide thermo-mechanical stability of ITER. Radioactive fuel may be stored in the gaps of castellated structures representing a safety issue for ITER.

Tungsten castellated structures with different shapes were exposed in TEXTOR to investigate the impact of cell shaping on impurity transport and fuel deposition in the gaps.

After exposure a significant intermixing of tungsten was detected in carbon deposits in the gaps reaching 70 at. % W in the deposition layer. This will provide difficulties in cleaning the gaps in ITER. Poloidal gaps of shaped cells contained a factor or 3 less deuterium than those of rectangular cells, the carbon deposition exhibited only marginal advantages of a new geometry. Poloidal and toroidal gaps contained comparable amount of C and D. Significant deposition at the bottom of gaps was measured which could only partly be reproduced by modeling.

PACS: 52.55.Fa; 52.40.Hf; 52.25.Vy

JNM Keywords: Plasma-material interactions (P0500), Surface effects (S1300), Carbon (C0100), Divertor materials (D0500); Cladding materials (C0500);

PSI 18 Keywords: Deuterium inventory, Erosion and Deposition, High-Z limiter, Tungsten, TEXTOR

Corresponding and presenting author: Dr. Andrey Litnovsky

Corresponding and presenting author address: Institut für Energieforschung - Plasmaphysik, Forschungszentrum Jülich, D-52425 Jülich, Germany

Corresponding and presenting author E-mail: a.litnovsky@fz-juelich.de

Introduction

The first wall and divertor armor in ITER will be castellated by splitting them into small-size cells to maintain the thermo-mechanical stability. There is a concern that the radioactive tritium will be accumulated in the gaps of the castellation representing a safety issue for ITER. Therefore the dedicated studies of the fuel accumulation in the gaps are ongoing on several facilities [1-3]. Investigations of deposits in the gaps of castellated structures are also important to assess the feasibility of cleaning of gaps, which might become necessary for continuation of ITER operation.

Dedicated research is ongoing in Forschungszentrum Jülich (Germany, EU) where the impurity transport and fuel inventory in the gaps, the behavior of castellated structures at extreme temperatures and cleaning of deposits in the gaps are being investigated [4-9]. In a recent experiment a tungsten limiter with two different shapes of castellation was exposed in the scrape-off layer (SOL) plasmas in TEXTOR. The aim of this experiment was to analyze the effect of shaping on the impurity and fuel transport to the gaps.

Experimental

The tungsten castellated limiter had a double roof form where the two types of cells were installed: rectangular cells with dimensions (10x10x15 mm) and the roof-like shaped cells with dimensions (10x10x12/15 mm). Each cell was mounted separately on the castellation holder (Fig. 1).

The limiter was introduced to TEXTOR using the limiter lock transport system [10] and exposed in the SOL plasmas at a radial distance R=46.8 cm, 0.8 cm further away from the Last Closed Flux Surface (LCFS). Sixteen neutral beam-heated discharges were made with total plasma duration of 112 seconds. Plasma parameters were monitored using a fast probe.

The bulk temperature of the limiter ranged between ~200°C-250°C as controlled with thermocouples. The temperature of the tungsten top surface was monitored via optical pyrometer. Castellated structures were exposed in the same plasma environment which was inferred from Hα measurements. In the end of exposure problems with the plasma control occurred causing a plasma shift towards the limiter, leading to the excursions of the surface temperature of tungsten up to 1500°C.

The nomenclature introduced earlier in [8] is remained (Fig. 1). The shaped cells faced the ion-drift direction are marked with "i"-letter, the rectangular cells were placed on the electron-drift direction and assigned with an "e" letter. There were 2 rows with 3 cells in the row for each shape of castellation. The rows were enumerated with 1 and 2 starting from the plasma-closest one. The cells were marked with letters "a" to "c" as shown on Fig. 1. The gaps elongated along the toroidal field direction are referred as the toroidal gaps, the poloidal gaps were named similarly.

Post-exposure analyses

After exposure all the cells were visually inspected. The top plasma-wetted tungsten surfaces were metallically shiny, whereas in all the gaps deposition patterns were observed. Sputter depth profiling by Secondary Ion Mass-Spectrometry (SIMS) was applied to toroidal and poloidal gaps, bottom surfaces of the gaps and top surfaces. The SIMS measurements were calibrated using DEKTAK stylus profiler. To determine the total areal density of carbon and deuterium, the line-scans using the Nuclear Reaction Analyses (NRA) technique were made on the side surfaces of both shaped and non-shaped cells utilizing a 1.2 MeV beam of ^{3}He ions. The Electron Probe MicroAnalysis (EPMA) measurements were made near to the NRA scans. The carbon concentration was inferred from an intensity of inner shell Kα electron emission.

Results

Tungsten intermixing in the deposits

Using special evaluation software for the EPMA measurements it was possible to recover the measured attenuation of the CKα emission and cross-correlate it with NRA and SIMS measurements which are insensitive to W intermixing. Such evaluation was made for toroidal and poloidal gaps. An example for a poloidal gap is provided on the figure 2. The calculation shows, that W fraction in the deposit is reaching about 70 at. % of W at the plasma-closest edge of the plasma-shadowed side of the gap. Such an intermixing will cause significant problems of cleaning deposits in the gaps. The W fraction in the deposit decreases with the depth of a gap rapidly reaching 2 at. % approximately 2 mm deeper in the gap. Much lower concentration of W was obtained for toroidal gaps reaching only about 10 at. %. at its maximum.

Deposition in poloidal gaps

Deposition patterns on the poloidal gaps of shaped and rectangular cells show remarkable differences: on the rectangular cells on the plasma-open side a thin shiny net erosion zone followed by the net deposition area deeper in the gap were detected, in agreement with earlier observations [4, 7]. On the contrary, only metallically shiny zone was observed on the plasma open sides of the shaped cells. For the non-shaped cells the deposition pattern was much more peaked at the plasma-closest edge of the gap reaching significantly higher maximum value than that for shaped cells (Fig. 3). The integration of the deposition profiles were made for both geometries of cells in order to get the total amount of carbon and deuterium in the gaps. The accuracy of this quantification is better than 20%.

The results are summarized in the table 1a. Significantly lower amount of D was found in the deposits of shaped cells, compared with that of rectangular ones. However, the amount of carbon in the gaps of both geometries was comparable outlining a need for the further optimization of shaping. The overall D/C ratio is not exceeding 0.03 which is due to the thermal excursions during the exposure.

Deposition in toroidal gaps

Similar measurements were made on toroidal gaps. The quantification of the deposition of carbon and deuterium was more difficult due to the complicated 2D deposition patterns. Results are outlined in the table 1b. Large differences in the total amounts of C and D were observed depending on the side of the gap: right or left from the magnetic field direction (Fig. 1). These differences were independent on the cell shaping: the deposition patterns on the toroidal cells located at the 'left' were very similar for shaped and rectangular cells and were drastically different from the patterns obtained on the 'right'. This implies, that the existing small misalignment of the gaps with respect to magnetic field direction could not be the major process leading to the observed deposition in these gaps. The most probable reason is the local shadowing of one side of toroidal gaps due to large gyroradii of the plasma and impurity ions compared to the gap width. Indeed, the calculated typical Larmor radii for the main plasma and impurity ions are of order of 1.5-2 mm whereas the gap size in our experiment is only 0.5 mm preventing charged particles from reaching one side of toroidal gap directly.

As can be seen from the table 1, toroidal gaps contain the comparable amount of deuterium as poloidal ones. The carbon amount stored in toroidal gaps is even higher than that in poloidal ones. This means that direct measurements of deposition in toroidal gaps are needed rather than extrapolation of the results from poloidal gaps.

Top surfaces

After exposure the top plasma-wetted surfaces of the castellation cells remained metallically shiny exhibiting an area of net erosion as confirmed by SIMS measurements, demonstrating that although the limiter was exposed under erosion-dominated conditions, deposition occurs in the gaps acting as a trap for impurities. On the shaped cells because of the geometry of shaping, an area shadowed from the plasma was created. On this area up to 40 nm-thick carbon deposits were measured with SIMS. These deposits were growing throughout the entire exposure time due to C transport into the shadowed area. However, the deposits were found to be completely covered with 150 nm-thick layer of W, having pure metallic appearance. The reason for this massive W deposition is in the enhanced erosion of the tungsten components because of plasma shifts in the end of exposure. Such a "protective" metal covering can also occur in ITER during e.g. transient effects making the cleaning of deposits even on top of castellation impossible.

Deposition at the bottom of the gaps

Deposition at the bottom of the gaps was detected on the holder of the castellation. SIMS measurements revealed up to 200 nm-thick deposits although no deposition was detected at the side walls of all the gaps close to their bottom. No tungsten intermixing has occurred in the deposits and no pronounced anisotropy in poloidal or toroidal directions was observed pointing out to the neutral origin of the deposition. Measurement show that about 14% of total amount of C deposited in the poloidal gaps were detected at their bottom. Similar patterns were observed after the recent long-term experiment, where micrometer-thick deposits were observed at the bottom of the gap between ALT limiter tiles in TEXTOR [11]. All these findings called for the significant re-assessment of the existing modeling algorithms.

Modeling of the deposition in the gaps

Earlier it was noted that simple processes of particle reflection from the gap walls might satisfactorily reproduce experimental deposition patterns [6]. The new findings such as deposition at the bottom of the gaps showed that the modeling algorithms must be improved. A new 3D program code was developed implementing an angular dependence of the reflection and neutral collisions inside the gap. Recently a simple treatment of chemical erosion processes together with a homogeneous surface mixing model was implemented in the code. Several modeling runs were made studying the relative effect of the aforementioned physical processes on the resulting simulated deposition pattern and compared with experimental one. In particular, an implementation of particle reflection at the different angles of incidence of impinging flux was not able to reproduce the experimental results. It was found that at given experimental conditions elastic collisions are very rare and have no significant effect on the deposition pattern, since the maximum pressure in the gap does not exceed 10^{-3} Bar. Finally, a simple description of chemical erosion with fixed erosion yields was implemented in the code which allowed a better agreement with an experiment assuming chemical erosion coefficient of Y=0.01 and a particle reflection coefficient of 0.9. These results are provided on figure 4, where the deposition at the side surfaces of a gap and at its bottom is plotted similar to the experimental data (Fig. 1). It can be seen that the new code does show better agreement with experimental data, yet still partial implying that important physics may still be missing.

Summary and outlook

Tungsten castellated limiter with the two shapes of the castellation was exposed in the SOL plasmas of TEXTOR to test the castellation shaping as a tool to mitigate the impurity

transport and fuel accumulation in the gaps. The limiter was exposed under erosion-dominated conditions, nevertheless deposition-dominated conditions occurred in the gaps.

Significant tungsten intermixing was observed reaching up to 70 at. % of W in the carbon deposited layers in the poloidal gaps. Metal intermixing will significantly decrease the efficiency of cleaning of gaps in ITER.

A factor of 3 less deuterium was found in the gaps of shaped poloidal cells compared with non-shaped ones. The difference in the carbon deposition was less pronounced, calling for the further optimization of shaping. Toroidal gaps contained comparable amount of carbon and deuterium and cannot be ignored from the accounting of fuel inventory and impurity transport in the gaps. Gaps contained about 10% of the total amount of carbon and less than 0.01% of deuterium impinging the castellation. Low trapping ratio for D may be caused by the temperature excursions during exposures.

Significant deposition was detected at the bottom of the gaps: up to 14% of the total amount of carbon deposited on poloidal gaps was found at their bottom.

Several new processes were introduced in the upgraded model to reproduce experimental results. However, only partial agreement of modeled patterns with the experimental data is achieved so far calling for further improvements.

Acknowledgments

The authors would like to thank M. Freisinger, H. Reimer, W. Müller and TEXTOR team for help and support. We are also grateful to Mrs. A. Stärk from the Central Department of Chemical Analyses of the Forschungszentrum Jülich for the SIMS data and to Mr. M. Spähn from RWTH Aachen for EPMA measurements. This work is being performed within the research program of the European Task Force on Plasma-Wall Interactions.

References:

1. K. Krieger, W. Jacob, D.L. Rudakov, R. Bastasz, G. Federici, A. Litnovsky, H. Maier, V. Rohde, G. Strohmayer, W.P. West, J. Whaley and C.P.C. Wong, J. Nucl. Mater., 363–365 (2007) 870;
2. D. Rudakov, W. Jacob, K. Krieger, A. Litnovsky, V. Philipps, W. P. West, C. P. C. Wong, S. L. Allen, R. J. Bastasz, J. A. Boedo, N. H. Brooks, R. L. Boivin, G. De Temmerman, M. E. Fenstermacher, M. Groth, E. M. Hollmann, C. J. Lasnier, A. G. McLean, R. A. Moyer, P. C. Stangeby, W. R. Wampler, J. G. Watkins, P. Wienhold and J. Whaley Phys. Scr. T128 (2007) 29;
3. M. Rubel, J. P. Coad, P. Wienhold, G. Matthews, V. Philipps, M. Stamp and T. Tanabe, Phys. Scripta T111 (2004), 112;
4. A. Litnovsky, V. Philipps, P. Wienhold, G. Sergienko, B. Emmoth, M. Rubel, U. Breuer and E. Wessel, J. Nucl. Mater. 337-339 (2002) 917;
5. A. Litnovsky, V. Philipps, P. Wienhold, G. Sergienko, A. Kreter, O. Schmitz, U. Samm, P. Karduck, M. Blome, B. Emmoth and M. Rubel Proc.of 32nd EPS Conf. ECA Vol.29C (2005) P-1.015;
6. A. Litnovsky, V. Philipps, A. Kirschner, P. Wienhold, G. Sergienko, A. Kreter, U. Samm, O. Schmitz, K. Krieger, P. Karduck, M. Blome, B. Emmoth, M. Rubel, U. Breuer and A. Scholl, J. Nucl. Mater., 367–370 (2007) 1481;
7. G. Sergienko, B. Bazylev, A. Huber, A. Kreter, A. Litnovsky, M. Rubel, V. Philipps, A. Pospieszczyk, Ph. Mertens, U. Samm, B. Schweer, O. Schmitz and M. Tokar, J. Nucl. Mater., 363–365 (2007) 96;
8. A. Litnovsky, V. Philipps, P. Wienhold, K. Krieger, G. Sergienko, A. Kreter, O. Schmitz, U. Samm, Ph. Mertens, A. Kirschner, S. Droste, S. Richter, U. Breuer, A. Scholl, A. Besmehn and Y. Xu, Phys. Scr. T128 (2007) 45;

9. A. Litnovsky, V. Philipps, P. Wienhold, K. Krieger, A. Kirschner, D. Borodin, G. Sergienko, O. Schmitz, A. Kreter, U. Samm and TEXTOR Team, S. Richter and U. Breuer, J. Nucl. Mater. in press.
10. B. Schweer, S. Brezinsek, H.G. Esser, A. Huber, Ph. Mertens, S. Musso, V. Philipps, A. Pospieszczyk, U. Samm, G. Sergienko and P. Wienhold, Fus. Sci. and Technology, Vol. 47, Nr. 2 (2005) 138;
11. A. Kreter, P. Wienhold, H. G. Esser, A. Litnovsky, V. Philipps, U. Breuer, S. Richter, K. Sugiyama, talk at the 10th meeting of the ITPA TG on Div. and SOL, Avila, Spain, January 2008.

Figures:

Figure 1. A view of a castellated limiter III after exposure with a nomenclature and geometry of cells and the scheme of exposure.

Figure 2. a) Estimated tungsten content (at. %) in the deposited layers formed in the poloidal gap of the rectangular cells and b) the appearance of deposition at the side walls of the shaped cells.

Figure 3: a) Distribution of areal deuterium and carbon atom density as determined by NRA along the depth of poloidal gap of the rectangular (er12a) and shaped (is12a) cells: 1) Carbon atom density distribution along the gap of rectangular cell; 2) Deuterium atom density distribution along the gap of rectangular cell; 3) Carbon atom density distribution along the gap of shaped cell; 4) Deuterium atom density distribution along the gap of shaped cell.

b) The gap geometry. Arrows show the direction of the line scan along the gap.

Figure 4. Modeling of impurity transport and fuel accumulation in the gaps: a deposition pattern on the poloidal gap obtained using a new algorithm.

Table 1. Total amount of D and C deposited on the poloidal and toroidal sides of gaps for both studied geometries: a) for poloidal gaps; b) for toroidal gaps.

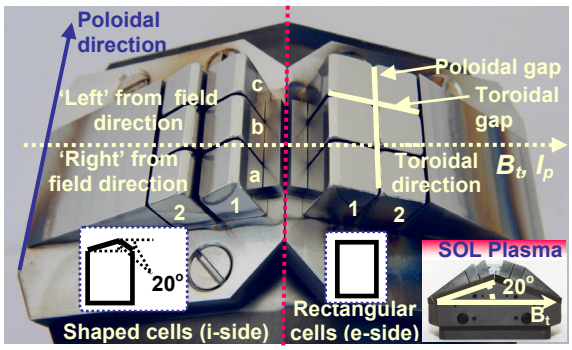

Figure 1: A view of a castellated limiter III after exposure with a nomenclature and geometry of cells and the scheme of exposure.

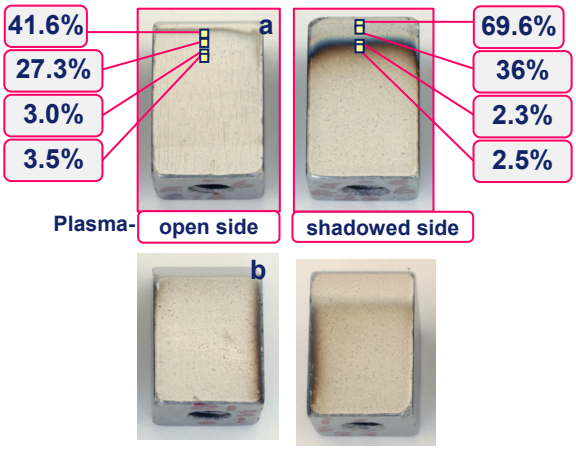

Figure 2. a) Estimated tungsten content (at. %) in the deposited layers formed in the poloidal gap of the rectangular cells and b) the appearance of deposition at the side walls of the shaped cells.

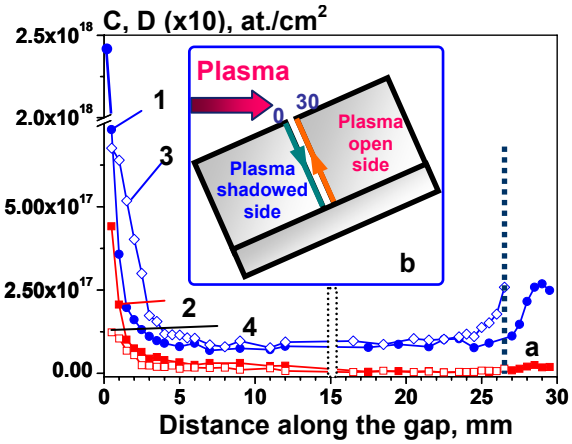

Figure 3: a) Distribution of areal deuterium and carbon atom density as determined by NRA along the depth of poloidal gap of the rectangular (er12a) and shaped (is12a) cells: 1) Carbon atom density distribution along the gap of rectangular cell; 2) Deuterium atom density distribution along the gap of rectangular cell; 3) Carbon atom density distribution along the gap of shaped cell; 4) Deuterium atom density distribution along the gap of shaped cell.

b) The gap geometry. Arrows show the direction of the line scan along the gap.

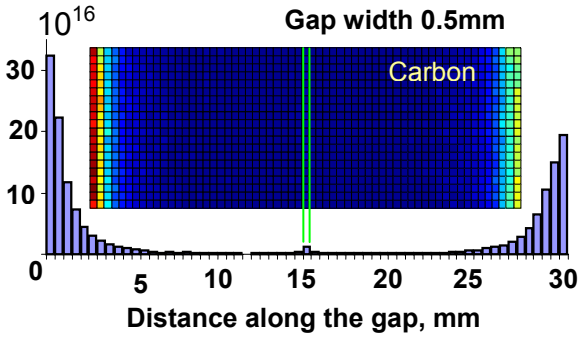

Figure 4. Modeling of impurity transport and fuel accumulation in the gaps: a deposition pattern on the poloidal gap obtained using a new algorithm.

Table 1.

a. Poloidal gaps				
Total integrated amount	Non-shaped cell	Shaped cell	Non-shaped cell	Shaped cell
	Plasma-open (A)	Plasma-open (A)	Plasma-shadowed (B)	Plasma-shadowed (B)
D, at.	$9.6*10^{14}$	$5.4*10^{14}$	$9.7*10^{15}$	$3.0*10^{15}$
C, at.	$1.4*10^{17}$	$1.1*10^{17}$	$2.1*10^{17}$	$2.0*10^{17}$
D/C, %	0.007	0.005	0.05	0.015
Ratio D_{rect}/D_{shaped} and C_{rect}/C_{shaped}	1.8/1.2		3.2/1.0	
b. Toroidal gaps				
	Left side	Left side	Left side	Left side
D, at.	$3.3*10^{15}$	$1.0*10^{15}$	$1.1*10^{16}$	$5.5*10^{15}$
C, at.	$2.5*10^{17}$	$1.3*10^{17}$	$2.0*10^{17}$	$2.0*10^{17}$
D/C	0.013	0.007	0.0055	0.027
Total integrated amount	Non-shaped cell First row	Shaped cell First row	Non-shaped cell Second row	Shaped cell Second row
	Right side	Right side	Right side	Right side
D, at.	$3.3*10^{15}$	$1.1*10^{15}$	$1.6*10^{16}$	$9.7*10^{15}$
C, at.	$4.0*10^{17}$	$2.8*10^{17}$	$2.8*10^{17}$	$4.5*10^{17}$
D/C	0.008	0.004	0.056	0.022

Table 1. Total amount of D and C deposited on the poloidal and toroidal sides of gaps for both studied geometries: a) for poloidal gaps, b) for toroidal gaps.